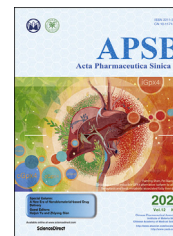




Chinese Pharmaceutical Association
Institute of Materia Medica, Chinese Academy of Medical Sciences

Acta Pharmaceutica Sinica B

www.elsevier.com/locate/apsb
www.sciencedirect.com



ORIGINAL ARTICLE

Combination therapy using microwave ablation and D-mannose-chelated iron oxide nanoparticles inhibits hepatocellular carcinoma progression



Rui Cui^{a,b,†}, Luo Wang^{a,†}, Dongyun Zhang^{a,†}, Kun Zhang^{c,d},
Jianping Dou^a, Linan Dong^a, Yixuan Zhang^a, Jiapeng Wu^a,
Longfei Tan^{e,*}, Jie Yu^{a,*}, Ping Liang^{a,*}

^aDepartment of Interventional Ultrasound, PLA General Hospital, Beijing 100853, China

^bDepartment of Medical Ultrasonics, the Sixth Affiliated Hospital, Sun Yat-sen University, Guangzhou 510655, China

^cLaboratory of Controllable Preparation and Application of Medical Ultrasound, Shanghai Tenth People's Hospital, Tongji University School of Medicine, Shanghai 200072, China

^dUltrasound Research and Education Institute, Tongji University School of Medicine, Shanghai 200072, China

^eLaboratory of Controllable Preparation and Application of Nanomaterials, Key Laboratory of Cryogenics, Technical Institute of Physics and Chemistry, Chinese Academy of Sciences, Beijing 100190, China

Received 17 April 2022; received in revised form 2 May 2022; accepted 11 May 2022

KEY WORDS

Microwave ablation;
Hepatocellular carcinoma;
Iron oxide nanoparticle;
Macrophage polarization;
Targeted therapy

Abstract Despite being a common therapy for hepatocellular carcinoma (HCC), insufficient thermal ablation can leave behind tumor residues that can cause recurrence. This is believed to augment M2 inflammatory macrophages that usually play a pro-tumorigenic role. To address this problem, we designed D-mannose-chelated iron oxide nanoparticles (man-IONPs) to polarize M2-like macrophages into the antitumor M1 phenotype. *In vitro* and *in vivo* experiments demonstrated that man-IONPs specifically targeted M2-like macrophages and accumulated in peri-ablation zones after macrophage infiltration was augmented under insufficient microwave ablation (MWA). The nanoparticles simultaneously induced polarization of pro-tumorigenic M2 macrophages into antitumor M1 phenotypes, enabling the transformation of the immunosuppressive microenvironment into an immunoactivating one. Post-MWA macrophage polarization exerted robust inhibitory effects on HCC progression in a well-established orthotopic liver

*Corresponding authors. Tel./fax: +86 10 66939530 (Jie Yu and Ping Liang), +86 10 82543521 (Longfei Tan).

E-mail addresses: longfeitan@mail.ipc.ac.cn (Longfei Tan), jiemi301@163.com (Jie Yu), liangping301@hotmail.com (Ping Liang).

[†]These authors made equal contributions to this work.

Peer review under responsibility of Chinese Pharmaceutical Association and Institute of Materia Medica, Chinese Academy of Medical Sciences

<https://doi.org/10.1016/j.apsb.2022.05.026>

2211-3835 © 2022 Chinese Pharmaceutical Association and Institute of Materia Medica, Chinese Academy of Medical Sciences. Production and hosting by Elsevier B.V. This is an open access article under the CC BY-NC-ND license (<http://creativecommons.org/licenses/by-nc-nd/4.0/>).

cancer mouse model. Thus, combining thermal ablation with man-IONPs can salvage residual tumors after insufficient MWA. These results have strong potential for clinical translation.

© 2022 Chinese Pharmaceutical Association and Institute of Materia Medica, Chinese Academy of Medical Sciences. Production and hosting by Elsevier B.V. This is an open access article under the CC BY-NC-ND license (<http://creativecommons.org/licenses/by-nc-nd/4.0/>).

1. Introduction

Thermal ablation is an internationally recognized first-line treatment for early-stage hepatocellular carcinoma (HCC)¹. Microwave ablation (MWA) is a thermal ablation technique that has been employed to treat HCC over the past 20 years. This method has several theoretical advantages, including fast heating, high temperature, and low susceptibility to heat-sink effects^{2,3}. However, progression and recurrence of residual tumors after ablation still occur when MWA is used on large tumors or when they are at a difficult location, thereby affecting the therapy outcome and long-term quality of life^{4,5}. This progression is attributable to insufficient thermal ablation and sterile inflammation around the coagulation necrosis area^{6–8}. Because MWA is a type of thermal ablation, it eradicates tumors by the coagulative necrosis of tumor cells. In the peripheral zone, which is adjacent to the central coagulative necrosis area, the heat-induced injury still occurs, but it is sublethal and reversible³. If MWA is insufficient, tumor residues would be left behind. In the peri-ablation zone, the upregulated expression of neovascularization-related genes can cause inflammatory reactions, including the secretion of growth factors or chemokines and recruitment of pro-tumorigenic M2 inflammatory macrophages. These responses inevitably induce repair processes⁹ and potentiate an immunosuppressive tumor microenvironment¹⁰. In particular, M2 macrophages mediate wound healing *via* extracellular matrix remodeling, angiogenesis, and immunosuppression^{9,11}. Thus, an increase in M2-type macrophage numbers in the tumor immune microenvironment contributes to the growth and dissemination of the residual tumor, causing poor prognosis among HCC patients¹². Therefore, reprogramming M2 macrophages is important for inhibiting tumor recurrence and improving prognosis after MWA^{13–20} but remains a challenging task¹³.

In this study, M2 macrophages were polarized to the antitumor M1 phenotype^{21,22} using—as an M2-macrophage ligand—PEGylated ultrasmall iron oxide nanoparticles (IONPs) with chelated D-mannose. We expected this polarization because IONPs produce reactive oxygen species (ROS) *via* the Fenton reaction, and studies have shown that ROS can trigger the M2-to-M1 transformation^{17,18}. An increase in M1 macrophage numbers should exert a robust antitumor effect against post-MWA residual HCC tumors (Scheme 1). More importantly, MWA can augment inflammation and recruit macrophages to the ablation zone^{23,24}. This ablated region becomes an M2 macrophage reservoir for generating more antitumor M1 macrophages after Fe₃O₄-induced polarization. We hypothesize that combining MWA-activated inflammation and macrophage polarization using D-mannose-chelated IONPs should effectively mitigate the immunosuppressive tumorigenic microenvironment and inhibit post-MWA tumor progression. Our findings provide evidence for the potential use of the proposed nanoparticles for cancer treatment.

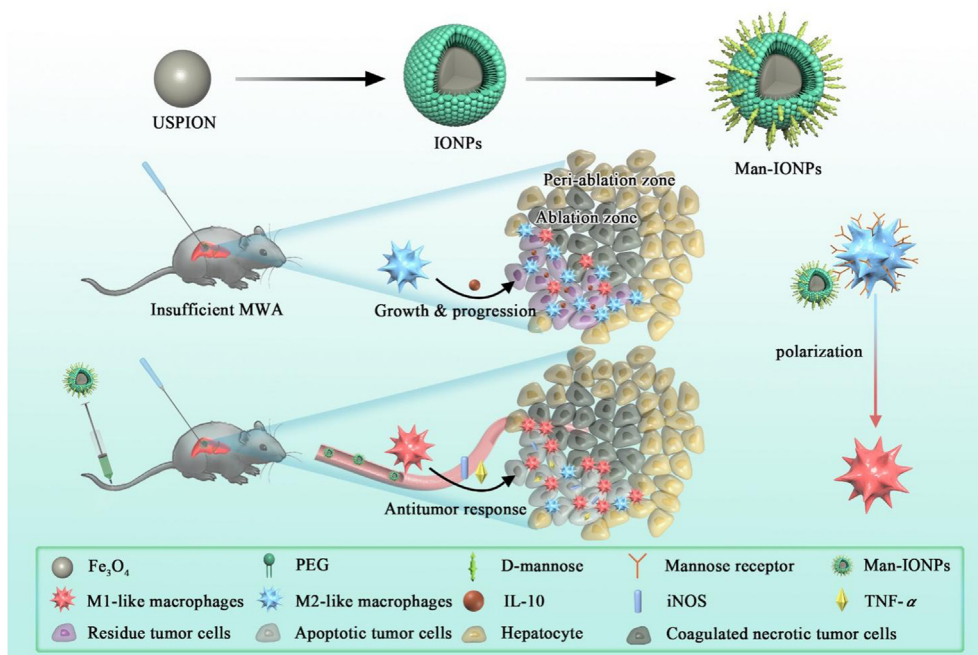
2. Materials and methods

2.1. Synthesis, cell viability assay, and acute toxicity assay of man-IONPs

D-Mannose-chelated IONPs (man-IONPs) were prepared as follows. First, 2 g of NaOH (Lan Yi Reagent, China) was mixed with 20 mL of DEG (J&K Scientific Ltd., Chengdu, China) (vacuum, 120 °C, 1 h) to prepare NaOH/diethylene glycol (DEG) solution. Next, 0.7 g of polyacrylic acid (J&K Scientific Ltd.) and 0.54 g of FeCl₃·6H₂O (Lan Yi Reagent) were dissolved in 15 mL of DEG, placed in a 220 °C vacuum for 30 min, and then mixed with 2 mL NaOH/DEG precursors before the reaction was incubated for another 10 min. This step generated uniformly distributed magnetic IONPs and the mixture was cooled to 25 °C. The samples were then dispersed in ethanol, centrifuged at 12,000 rpm for 10 min, dispersed again in deionized water, and washed 2–3 times. To synthesize man-IONPs, 6 mL nanoparticles (10 mg/mL) and 30 mg amino PEG (Lan Yi Reagent, China) were added into 24 mL of an aqueous solution containing 1.2 mL of EDC [N-(3-(dimethylamino) propyl)-N'-ethylcarbodiimide hydrochloride, J&K Scientific Ltd.] and 1.2 mL of NHS (N-hydroxysuccinimide, J&K Scientific Ltd.). After agitating for 3 h, 60 mg of D-mannose (J&K Scientific Ltd.) was added, and the reaction was continued overnight with continuous agitation. The solution was centrifuged at 12,000 rpm for 10 min and washed three times with deionized water to collect man-IONPs.

The cytotoxicity of man-IONPs on RAW264.7 cells and Hepa 1-6 cells (Cell Bank of the Chinese Academy of Sciences, Shanghai, China) was examined using CCK-8 assays. First, 100 μL RAW264.7 cells and Hepa 1-6 cells were cultured in 96-well plates (1 × 10⁵ cells/well) for 24 h. Next, 100 μL of man-IONP or IONP dispersions at varying Fe concentrations (10, 20, 50, 100, and 250 μg/mL) was added separately into each well and incubated for another 24 h. The medium was discarded, and wells were washed three times with phosphate-buffered saline (PBS). A new culture medium (100 μL) containing 10% CCK-8 (Beyotime Biotechnology, Shanghai, China) was added to each well and incubated for 1 h. Subsequently, absorbance at 450 nm was measured using a multi-functional microplate reader. Cell viability per group was calculated as a percentage of that in the control group.

For *in vivo* acute toxicity assays, healthy C57/BL6 mice aged 5–6 weeks were randomly divided into seven groups (*n* = 3 in each group). They were subjected to tail vein injections of man-IONPs or IONPs at three concentrations (5, 10, and 20 mg/kg Fe), or 5% glucose as control. Bodyweight was recorded for animals in each group. After 14 days, mice were euthanized, and blood was collected for biochemical tests. Organs including the liver, heart, spleen, lungs, and kidneys were extracted, and paraffin-embedded sections were prepared for hematoxylin-eosin staining.



Scheme 1 D-Mannose-chelated iron oxide nanoparticle (man-IONP) synthesis and principles of MWA and man-IONP combination therapy.

2.2. Animal model establishment

C57/BL6 male mice (5–6 weeks old) were purchased from SPF Biotechnology Company (Beijing, China) and housed in a specific pathogen-free room. All animal protocols in this study were approved by the Research Animal Care and Use Committee of the Chinese PLA General Hospital (approval number: 2017-X13-52, Beijing, China) and are in line with the American Association for Laboratory Animal Science (AALAS) guidelines. All procedures were conducted under aseptic conditions and isoflurane anesthesia. To establish a mouse model of orthotopic liver cancer, 25 μ L of a mixture containing Hepa 1-6 cells (Cell Bank of the Chinese Academy of Sciences) and Matrigel (Basement Membrane Matrix 356234, Corning, USA) was injected into the center of the left hepatic lobe. One week later, when the maximum diameter of liver tumors reached 7–9 mm, mice were anesthetized, and a laparotomy was performed.

These mice were then subjected to low levels of MWA (insufficient for full tumor eradication) on a microwave ablation apparatus, with an antenna having an active tip length of 5 mm (Canyou Medical, Nanjing, China). The antenna was placed in the non-central site of liver tumors and set to an output power of 2 W for 1 min. At 2 weeks post-ablation, mice were sacrificed, and the ablated liver lobe was isolated for histopathological examination to assess macrophage recruitment.

2.3. Evaluating targeting and polarization effects using man-IONPs

To mimic M1 and M2 macrophage phenotypes, bone marrow-derived macrophages (BMDM) were cultured. The bone marrow was harvested from femurs of 5–6-week-old C57/BL6 mice and filtered through a 70- μ m mesh filter (SPL Life science, USA). The cell suspension was immediately centrifuged at 500 \times g for 5 min, resuspended in complete medium containing M-CSF (40 ng/mL) (PeproTech, USA), pipetted onto 6-well plates, and cultured at

37 $^{\circ}$ C in a 5% CO₂ incubator. After 6 days, The six-well plates were washed with RPMI 1640 medium (Hyclone, GE healthcare life science, USA) and treated for 24 h with mouse recombinant IFN- γ (20 ng/mL, PeproTech, USA) and LPS (100 ng/mL) (Solarbio Science & Technology Co., Beijing, China) or recombinant mouse IL-4 (20 ng/mL) and IL-13 (20 ng/mL) (PeproTech), then yielded M1- and M2-like macrophages respectively. For IONPs and Man-IONPs groups, after 6 days of culture with complete medium containing M-CSF, the macrophages were incubated for 24 h with IONPs or Man-IONPs at a Fe concentration of 50 μ g/mL, as well as IL-4 and IL-13.

Quantitative reverse-transcription polymerase chain reaction (qRT-PCR) and enzyme-linked immunosorbent assay (ELISA) were performed to verify M1- and M2-like polarization induced by cytokines or man-IONPs. To perform qRT-PCR, macrophages were harvested, followed by RNA extraction using the RNA isolation kit (DP430, Tiangen Biotech, Beijing, China) according to the manufacturer's protocol. Thereafter, 1 μ g of total RNA was reverse-transcribed into complementary DNAs using a TIAN-Script RT kit (KR104-02, Tiangen Biotech). qRT-PCR was performed using primers described previously^{25–27} and a QuantStudio Dx Real-Time PCR Instrument (Thermo Fisher Scientific, USA) and FastFire qPCR PreMix kit (FP207-02, Tiangen Biotech). Primer sequences are shown in [Supporting Information Table 1](#). Cycling conditions were as follows: initial denaturation at 95 $^{\circ}$ C for 1 min, followed by 40 cycles at 95 $^{\circ}$ C for 20 s and 60 $^{\circ}$ C for 20 s mRNA expression was determined using the comparative Ct method. To further confirm the production of the M1 marker TNF α and the suppression of the M2 marker IL-10, ELISA assays were performed using mouse TNF and IL-10 ELISA kits (Biolegend, San Diego, CA, USA) following the manufacturer's instructions.

We performed Prussian blue staining to assess the targeting ability of man-IONPs. After M1- or M2-like macrophages were incubated with man-IONPs (50 μ g/mL Fe) for 6, 12, and 24 h, the percentages of iron-positive cells were calculated. For *in vivo*

experiments, the livers of C57/BL6 mice were subjected to MWA at an output power of 2 W for 1 min. After 2 weeks, IONPs or man-IONPs (20 mg/kg Fe) were injected into mouse tail veins. Animals were euthanized at 2, 6, and 12 h post-injection. Paraffin sections of ablated mouse livers were stained with Prussian blue to calculate the percentage of iron-positive cells in the peri-ablation zone.

Besides, inductively coupled plasma mass spectrometry (ICP-MS) was performed to test the Fe content of the treated liver lobe. At 12 h post-injection of IONPs, man-IONPs (20 mg/kg Fe), or 5% glucose, the mice were sacrificed, and the treated liver lobes were collected. After recording their weights, the liver tissue was digested with nitric acid, the solution was diluted, and tested with ICP-MS (Agilent 7800, Agilent Technologies, Japan).

2.4. Inhibition of local tumor progression after MWA

The mice with liver cancer were randomly divided into Group A: MWA only; Group B: tail vein injection of man-IONPs at 3 days, 1 week, and 2 weeks after MWA; Group C: tail vein injection of IONPs at 3 days, 1 week, and 2 weeks after MWA; and Group D: Control ($n = 3$ per group).

Magnetic resonance imaging (MRI) (7.0 T small animal MRI, TE: 40 ms, TR: 3000 ms, thickness: 1 mm, BioSpec70/20USR, Bruker, Germany) was performed to evaluate tumor growth in groups A, B, C, and D during pre-MWA, 1-week post-MWA, and 3 weeks post-MWA. Mice were euthanized 4 weeks post-MWA. Ablated livers were processed, and paraffin-embedded sections were prepared for immunocytochemistry and immunofluorescence staining.

To analyze immunohistochemical staining results, at least 3–5 visual fields were randomly selected to image the area between the normal ablation area and the non-ablation part of the liver in each section of each group. The same background light parameters were used for all photographs. Image-pro Plus 6.0 software was used for cell count analysis.

Flow cytometry analysis was performed to assess the M2 macrophages infiltration in groups A, B, and C. The treated liver tissues were minced using a surgical blade and incubated for 30 min in

DMEM (Invitrogen, USA) with 2.0 mg/mL Collagenase A (Roche, Switzerland) and 50 units/mL DNase I (Roche) at 37 °C. Single-cell suspensions were prepared by filtering them through a 70- μ m mesh filter (SPL Life science, USA). Thereafter, the cells were incubated for 15 min on ice with Fc Receptor Binding Inhibitor (BioLegend, USA) diluted 1:10 in PBS containing Zombie-Aqua fixable viability stain (BioLegend). The cells were then incubated for 30 min in PBS containing 1.0 mmol/LEDTA and 5% FCS along with the dilutions of fluorescently-labeled primary monoclonal antibodies for surface markers. The following antibodies were used: anti-CD45-Brilliant Violet 510™, anti-F4/80-PE, anti-CD86-APC-A750, anti-CD11c-PC5.5, and anti-CD11b-FITC (BioLegend). Thereafter, the cells were incubated in permeabilization solution (True-Nuclear™ 1X Fix Concentrate, BioLegend) at room temperature in the dark for 60 min. APC-conjugated anti-mouse CD206 (BioLegend) was then added and incubated for 30 min in the dark at room temperature. The acquisition was then performed using a flow cytometer (Beckman Coulter, USA). Data were analyzed using FlowJo Version 9.6.4. Live singlets were gated using FSC-H/FSC-A. M2 macrophages were identified as F4/80^{high}CD206^{high} cells.

2.5. Statistical analysis

Statistical analysis was performed using the GraphPad Prism 9.3.1.0 software. Comparison between the two groups was performed using an unpaired two-tailed Student's *t*-test. For comparison of multiple groups, one-way ANOVA was used, followed by Tukey's honest significant difference posthoc test or Bonferroni's multiple comparisons post-test, except when noted otherwise. Results are expressed as means \pm SD. A *P*-value of <0.05 was considered statistically significant.

3. Results

3.1. Preparation and biosafety evaluation of man-IONPs

Synthesis of IONPs and man-IONPs involved generating ultra-small superparamagnetic iron oxide nanoparticles (USPIONS) using a classic solvent thermal method^{28,29}, followed by

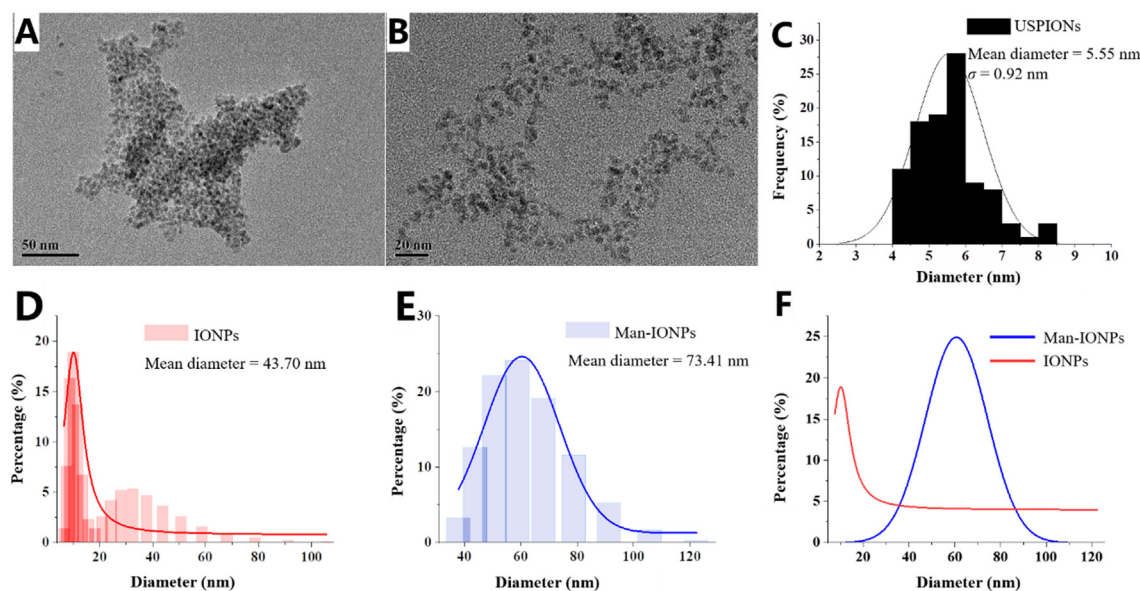


Figure 1 Characteristics of man-IONPs. (A, B) Transmission electron microscopic images of ultra-small superparamagnetic iron oxide nanoparticles USPIONS. (C–F) Particle size distributions of USPIONS, IONPs, and Man-IONPs.

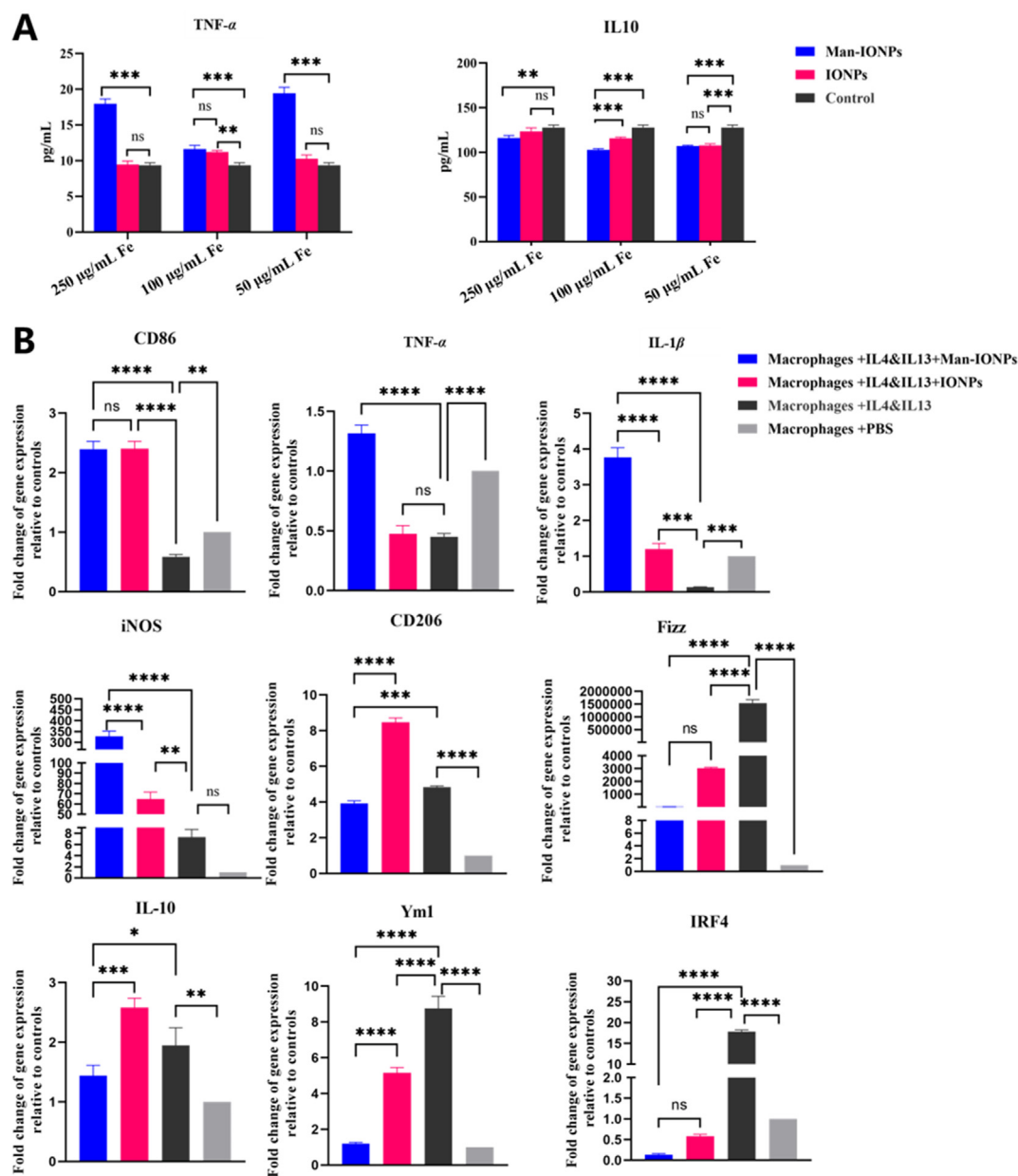


Figure 2 M2-like macrophage polarization by man-IIONPs. (A) ELISA results showing the secretion of TNF- α (M1-related marker) and IL-10 (M2-related marker) in M2-like macrophages as a function of IONP or man-IIONP concentrations. (B) Real-time PCR showing the expression of M1-related markers (CD86, TNF- α , IL-1 β , and iNOS) and M2-related markers (CD206, Fizz, IL-10, Ym1, and IRF4) in macrophages in response to different nanoparticle treatments conditions; dose of IONPs or man-IIONPs: 50 μ g/mL Fe. Data are expressed as mean \pm standard deviation (SD), $n = 3$; * $P < 0.05$, ** $P < 0.01$, *** $P < 0.001$, **** $P < 0.0001$.

sequential PEG and D-mannose conjugation (Scheme 1). Transmission electron microscopy (TEM) images of USPIONs exhibited a well-defined morphology (Fig. 1A and B); after measuring over 100 nanoparticles, the average size was determined as 5.55 ± 0.92 nm (Fig. 1C). Dynamic light scattering measurements showed that the average size of man-IIONP was larger (73.41 nm) than that of IONP (43.10 nm) because of D-mannose conjugation (Fig. 1D–F). Cytotoxicity experiments showed that after 24 h incubation with 0–100 μ g/mL Fe man-IIONPs, both Hepa 1–6 cells and RAW264.7 cells exhibited >80% viability, proving

the biosafety of these nanoparticles (Supporting Information Fig. S1).

Acute toxicity tests *in vivo* revealed that at 2 weeks post-injection of man-IIONPs or IIONPs (10 and 20 mg/kg Fe), routine blood test indicators (Supporting Information Fig. S2) and biochemical indicators (Supporting Information Fig. S3) were within the normal range. Hematoxylin-eosin staining of the heart, liver, spleen, lungs, and kidneys revealed no abnormalities in mice treated with man-IIONPs or IIONPs (doses: 10 and 20 mg/kg Fe) compared with those in the control group (Supporting Information Fig. S4).

3.2. *In vitro* M1-like polarization using man-IONPs

Recent years have seen an upsurge in chemodynamic therapy based on Fe-based nanoparticles, which leads to the Fenton reaction that produces ROS^{15,30}, thereby steering M2-to-M1 macrophage polarization^{17–22}. Here, we confirmed the ability of man-IONPs to polarize M2 macrophages into M1 macrophages by monitoring M1- and M2-related markers using ELISA and qRT-PCR. We first performed qRT-PCR to assess M1 and M2 polarization in cytokine-treated bone marrow-derived macrophages *in vitro*. Expectedly, these macrophages were induced into M1-like and M2-like macrophage phenotypes (Supporting Information Fig. S5). After IONP or man-IONP treatment, we measured IL-10 and TNF- α levels in M2-like macrophages by performing ELISA. We found that in the Fe concentration ranging from 50 to 100 $\mu\text{g/mL}$, the levels of IL-10 secretion in the man-IONPs group and IONPs group were significantly lower than those in the control group, whereas, in the Fe concentration of 100 $\mu\text{g/mL}$, IL-10 level in the man-IONPs group was lower than that in the IONPs group (Fig. 2A). Besides, in the Fe concentration ranging from 50 to 250 $\mu\text{g/mL}$, the levels of TNF- α in the man-IONPs group were significantly higher than those in the control group (Fig. 2A).

The qRT-PCR analysis revealed that Man-IONPs-exposed macrophages significantly upregulated the levels of M1-related CD86, TNF- α , IL-1 β , and iNOS markers (Fig. 2B) compared with macrophages only ($P < 0.05$). In addition, the mRNA levels of

M2-related CD206, Fizz, IL-10, Ym1, and IRF4 markers were significantly decreased after exposure to Man-IONPs ($P < 0.05$). Its polarization effect outperformed IONPs in terms of CD86, TNF- α , IL-1 β , iNOS, CD206, IL-10, and Ym1 markers ($P < 0.05$). These results indicated that man-IONPs facilitated M2 polarization to M1.

3.3. M2 macrophage targeting ability of man-IONP *in vitro* and the peri-ablation zone *in vivo*

We first performed Prussian blue staining to evaluate IONP uptake by macrophages *in vitro*. At 6, 12, and 24 h post-incubation, more man-IONPs entered the induced M2-like macrophage cells than IONPs (Fig. 3A). In particular, the M2 macrophage took up a larger amount of man-IONPs than of IONPs (percentage of positive cells, man-IONPs vs. IONPs: 6 h, $5.5 \pm 4.0\%$ vs. $0.3 \pm 0.3\%$, $P < 0.01$; 12 h, $5.7 \pm 1.6\%$ vs. $0.9 \pm 0.7\%$, $P < 0.01$; 24 h, $17.7 \pm 8.7\%$ vs. $4.6 \pm 2.5\%$, $P < 0.05$; Fig. 3C). In addition, at 24 h, M2 macrophages exhibited far higher man-IONP uptake than M1 macrophages (percentage of positive cells, M2 vs. M1, $20.3 \pm 10.0\%$ vs. $7.9 \pm 3.1\%$, $P < 0.05$; Supporting Information Fig. S6). This result demonstrates that chelated D-mannose ligands improve the specific M2-macrophage-targeting ability of man-IONPs, thereby facilitating M2-to-M1 polarization.

To verify the targeting ability of man-IONPs *in vivo*, we injected man-IONPs into the tail veins of C57BL mice 2 weeks

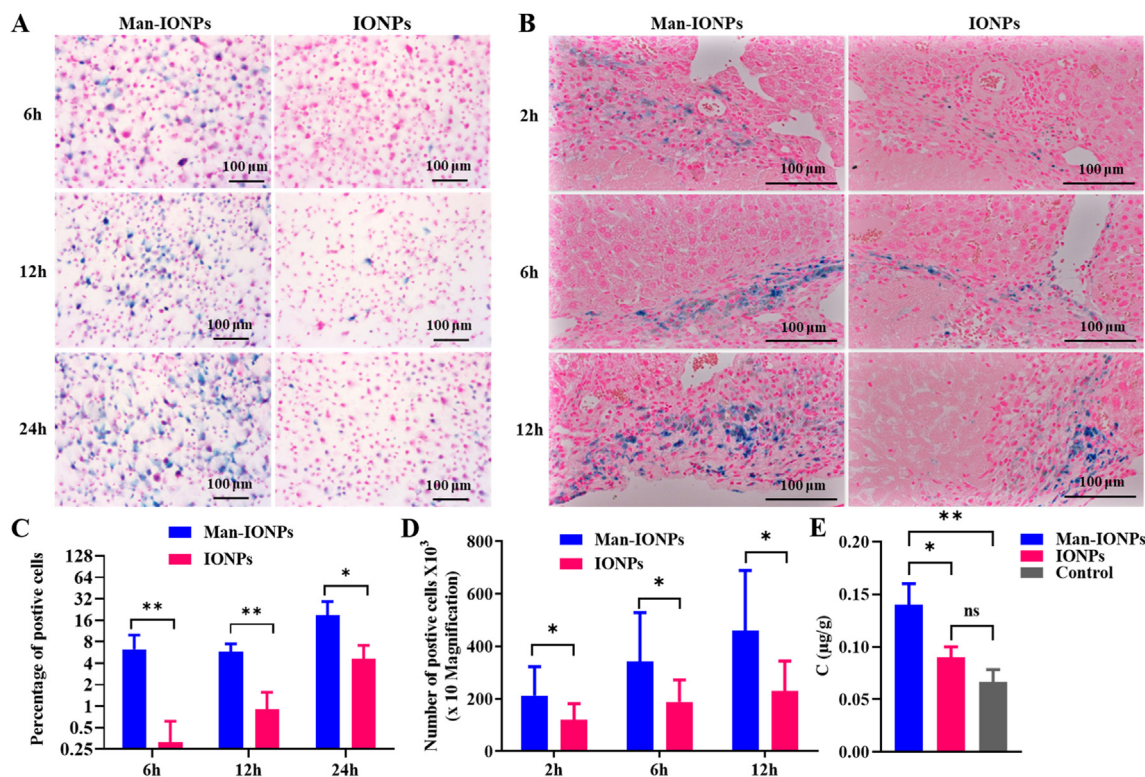


Figure 3 M2-like macrophages targeting by man-IONPs. (A) Microscopic images of Prussian blue-stained M2-like macrophages after incubation with man-IONPs or IONPs, the dose of IONPs or man-IONPs: 50 $\mu\text{g/mL}$ Fe. (B) Histological images of ablated liver sections stained with Prussian blue after tail vein injection of man-IONPs or IONPs. (C) The relative quantitative value of stained iron-positive cells in M2-like macrophages after various incubation periods. (D) Relative quantitative values of stained iron-positive cells in ablated liver sections after tail vein injection of man-IONPs or IONPs. (E) ICP-MS analysis of Fe content in ablated liver lobe, post-injection of man-IONPs, IONPs, or 5% Glucose. Data are expressed as mean \pm standard deviation (SD), $n = 3$; * $P < 0.05$, ** $P < 0.01$.

post-MWA. Histological examinations of ablated livers showed that in the peri-ablation zone, cells in the man-IONP group had significantly more positive iron stains than cells in the IONP group at 2, 6, and 12 h post-injection (number of positive cells, $\times 10^3$ per 10-fold vision field, man-IONPs vs. IONPs: 2 h, 219.7 ± 113.5 vs. 122.2 ± 63.4 , $P = 0.02$; 6 h, 387.2 ± 250.3 vs. 188.8 ± 92.2 , $P = 0.02$; 12 h, 414.9 ± 159.1 vs. 260.8 ± 93.1 , $P = 0.04$; Fig. 3B and D). Besides, according to the ICP-MS test of iron, in the post-MWA liver tissue at 12 h post-injection, the Fe content was higher in the man-IONPs group than that in the IONPs group (iron content, $\mu\text{g/g}$, 0.139 ± 0.017 vs. 0.090 ± 0.010 , $P = 0.01$; Fig. 3E).

3.4. Tumor progression and macrophage recruitment in the post-MWA peri-ablation zone

Two weeks after treatment with low-level MWA, the incidence of tumor progression was 100% (6/6) in our mouse model of orthotopic liver cancer. Local lesions were 4.1, 4.5, 7.2, 6.2, 5.3, and 6.6 mm in diameter, with an average diameter of 5.7 ± 1.1 mm (Fig. 4A). Immunohistochemical staining revealed that infiltrated macrophages around the ablation site gradually increased from 3 days to 2 weeks after MWA (Fig. 4B). At 2 weeks post-MWA, the number of CD68-positive cells per field was markedly higher than that at 3 days post-ablation (number of positive cells, $\times 10^3$ per 20-fold vision field, 2 weeks vs. 3 days, 46.6 ± 28.4 vs. 2.4 ± 2.5 , $P < 0.001$) and 1 week (2 weeks vs. 1 week, 46.6 ± 28.4 vs. 18.6 ± 15.5 , $P < 0.001$; Fig. 4C). Besides, the number of Ki-67 positive cells also increased within 2 weeks after ablation (Fig. 4C). Immunofluorescence staining showed that in the peri-ablation zone, the proportion of

green fluorescence-labeled M2-like macrophages was larger at 2 weeks after MWA than at 1 week after MWA (Fig. 4D).

3.5. Treatment with man-IONPs inhibited tumor progression after MWA

Since the resolution of MRI and fluorescence imaging is comparable, we performed MRI to monitor post-MWA tumor growth in four treatment groups (Fig. 5A). The pre-MWA volume of liver tumors in all groups was approximately identical ($P = 0.897$, Fig. 5B). After MWA, the ablated lesion expands because of coagulation necrosis. If the tumor is completely eradicated, it will be absorbed and its volume will be reduced. However, if thermal ablation is insufficient, the tumor will progress^{31,32}, and its volume will further increase. Therefore, 1 week after MWA, tumor size in all groups increased slightly (Fig. 5B). At 3 weeks after ablation, tumors in the MWA group remained the same in terms of size and hyperintense nodules were visible around the ablation area (Fig. 5A). However, tumors decreased in size or even disappeared in the MWA + man-IONP and MWA + IONP groups (Fig. 5B). Furthermore, the volume reduction rate in the MWA + man-IONP group was higher than that in the MWA + IONP group (0.88 ± 0.04 vs. 0.39 ± 0.29 , $P = 0.043$, Fig. 5C). Moreover, at 4 weeks post-ablation, the mice in the MWA group that had their liver ablated presented single or multiple nodules near the ablated area (Fig. 5D and E), whereas obvious tumor growth was absent near the ablation area in the MWA + man-IONP and the MWA + IONP groups (Fig. 5D and E).

Subsequently, we investigated whether man-IONPs inhibited macrophage recruitment in the post-MWA peri-ablation zone *in vivo*. At 4 weeks post-ablation, the MWA + man-IONP group

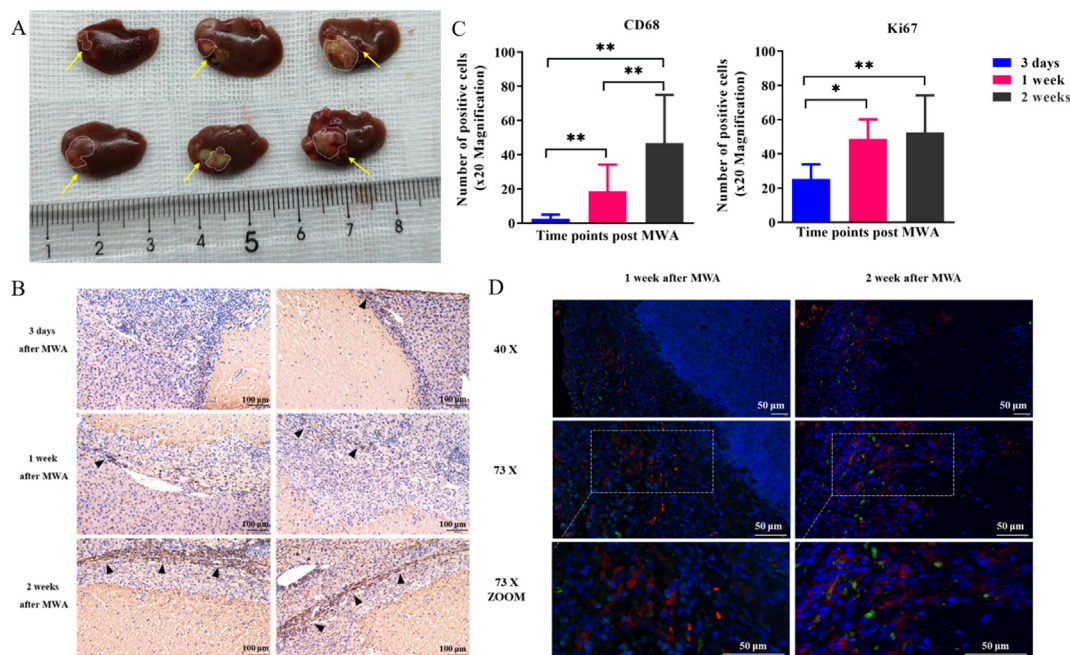


Figure 4 *In vivo* exploration of the variation trend of macrophages in the tumorigenic microenvironment after MWA. (A) Local tumor progression in the mouse model of orthotopic liver cancer at 2 weeks after low-level MWA treatment (yellow arrow indicates ablation area, the white dotted area shows local tumor progression). (B) Immunohistochemical staining of the ablated mouse liver lobe at 3 days, 1 week, and 2 weeks post-MWA, monitoring infiltrated CD68+ macrophages. (C) Relative secretion of different markers in the peri-ablation zone at 3 days, 1 week, and 2 weeks after MWA; data are expressed as mean \pm SD ($n = 3$), and $*P < 0.05$, $**P < 0.01$. (D) Immunofluorescence staining images of all infiltrated macrophages (CD68+, red) and M2-like macrophages (CD206+, green) in the peri-ablation zone at 1 week and 2 weeks after MWA. Scale bar: 50 μm .

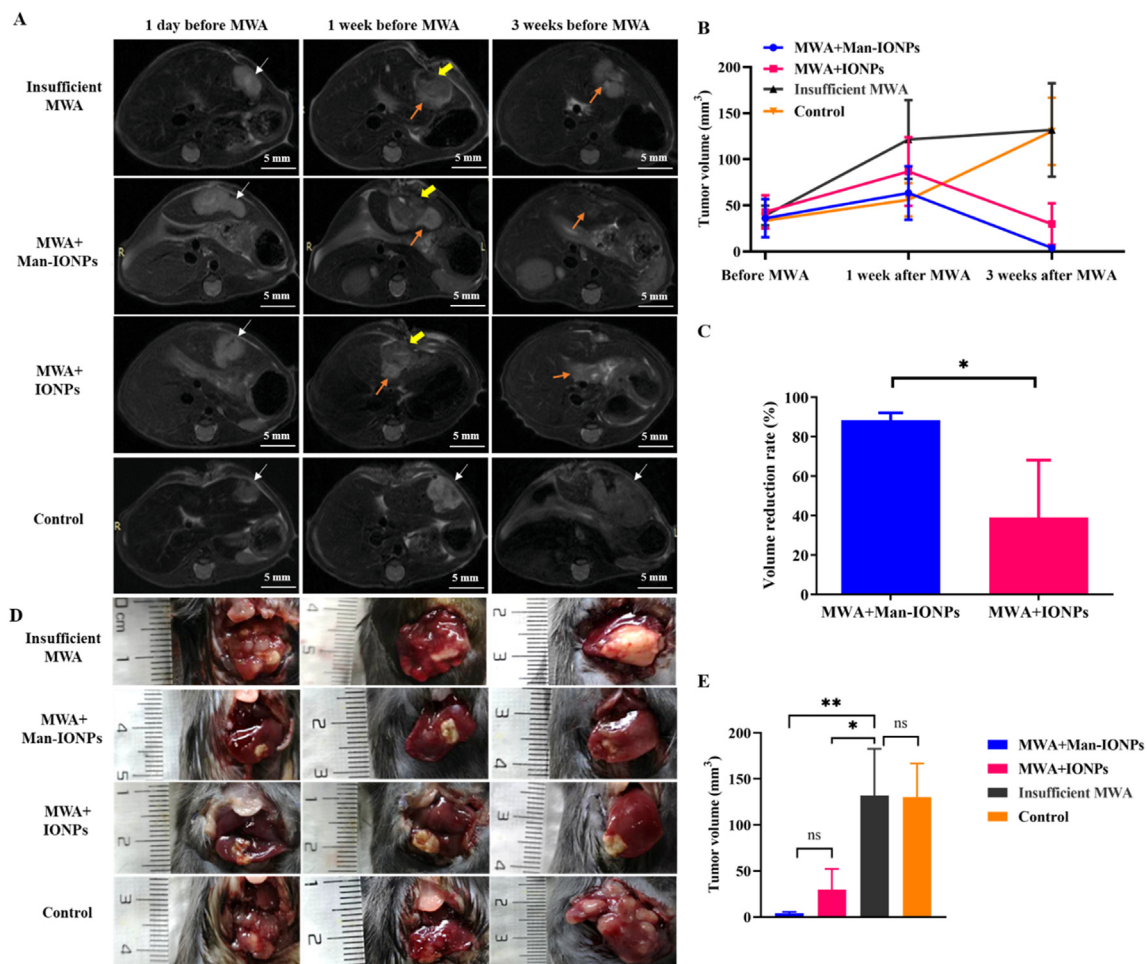


Figure 5 Evaluating man-IONP-mediated inhibition of tumor progression after MWA. (A) Time-dependent T2-weighted MRI images of ablated liver tumors in mice that underwent different treatments (white arrow indicates tumor area, yellow arrow shows ablation area, orange arrow shows local tumor progression). (B) Time-dependent variation in the liver tumor volume of mice that underwent different treatments. (C) The volume reduction rate of ablated liver tumors in mice that underwent MWA combining IONPs or man-IONPs at 3 weeks post-MWA. (D) Digital photos of local tumor progression after different incubation periods in various treatment groups. (E) Terminal volumes of liver tumors after 4 weeks of treatment in various treatment groups. Data are expressed as mean \pm SD ($n = 3$); * $P < 0.05$, ** $P < 0.01$.

had far lower counts of CD68-positive macrophages around the ablation area than the MWA + IONP (number of positive cells, $\times 10^3$ per 20-fold vision field, 7.2 ± 3.7 vs. 17.1 ± 10.8 , $P = 0.027$) and MWA (number of positive cells, $\times 10^3$ per 20-fold vision field, 7.2 ± 3.7 vs. 18.1 ± 13.3 , $P = 0.048$) groups (Fig. 6A). In addition, both the MWA + man-IONP and MWA + IONP groups (Fig. 6A) had notably fewer Ki-67-positive cells than the MWA group (number of positive cells, $\times 10^3$ per 20-fold vision field, MWA + man-IONPs vs. MWA, 112.3 ± 109.5 vs. 282.4 ± 118.7 , $P = 0.007$; MWA + IONPs vs. MWA, 79.1 ± 50.7 vs. 282.4 ± 118.7 , $P = 0.002$), demonstrating that the MWA + man-IONP treatment significantly inhibited the proliferation of residual tumor cells. After immunofluorescence staining, laser confocal scanning microscopic observations traced the infiltration of M2-like macrophages around the ablation zone. The MWA + man-IONP group had a lower proportion of M2-like macrophage (CD206⁺) infiltration around the ablation zone than the MWA and MWA + IONP groups (Fig. 6B).

The infiltration of M2-like macrophages in MWA, MWA + man-IONPs, and MWA + IONPs groups were evaluated by flow cytometry analysis. The results revealed decreased quantities of F4/

80^{high}CD206^{high} macrophages in MWA + man-IONPs and MWA + IONPs treated mice compared with mice only undergoing MWA (Fig. 6C and D). Moreover, the percentage of F4/80^{high}CD206^{high} macrophages was lower in MWA + man-IONPs than in MWA + IONPs (MWA + man-IONPs vs. MWA + IONPs, $2.1 \pm 1.7\%$ vs. $5.3 \pm 0.8\%$, $P = 0.043$, Fig. 6D).

4. Discussion

Several pre-clinical studies have focused on immunotherapy targeting TAMs, especially in the field of nanomedicine. One such study revealed that IONPs inhibit tumor growth by inducing macrophage polarization¹⁷. Therefore, the use of IONPs for suppressing tumor growth in clinical practice is promising. This study provides insights into the possible clinical scenario of IONPs as adjuvant therapy of MWA for liver cancer.

The feasibility of the combined use of MWA and IONPs against liver cancer is based on the phenomenon that macrophages' infiltration increases after MWA, which has been reported in a previous study⁷. However, the association between infiltrating macrophages and tumor progression was unclear. Our study

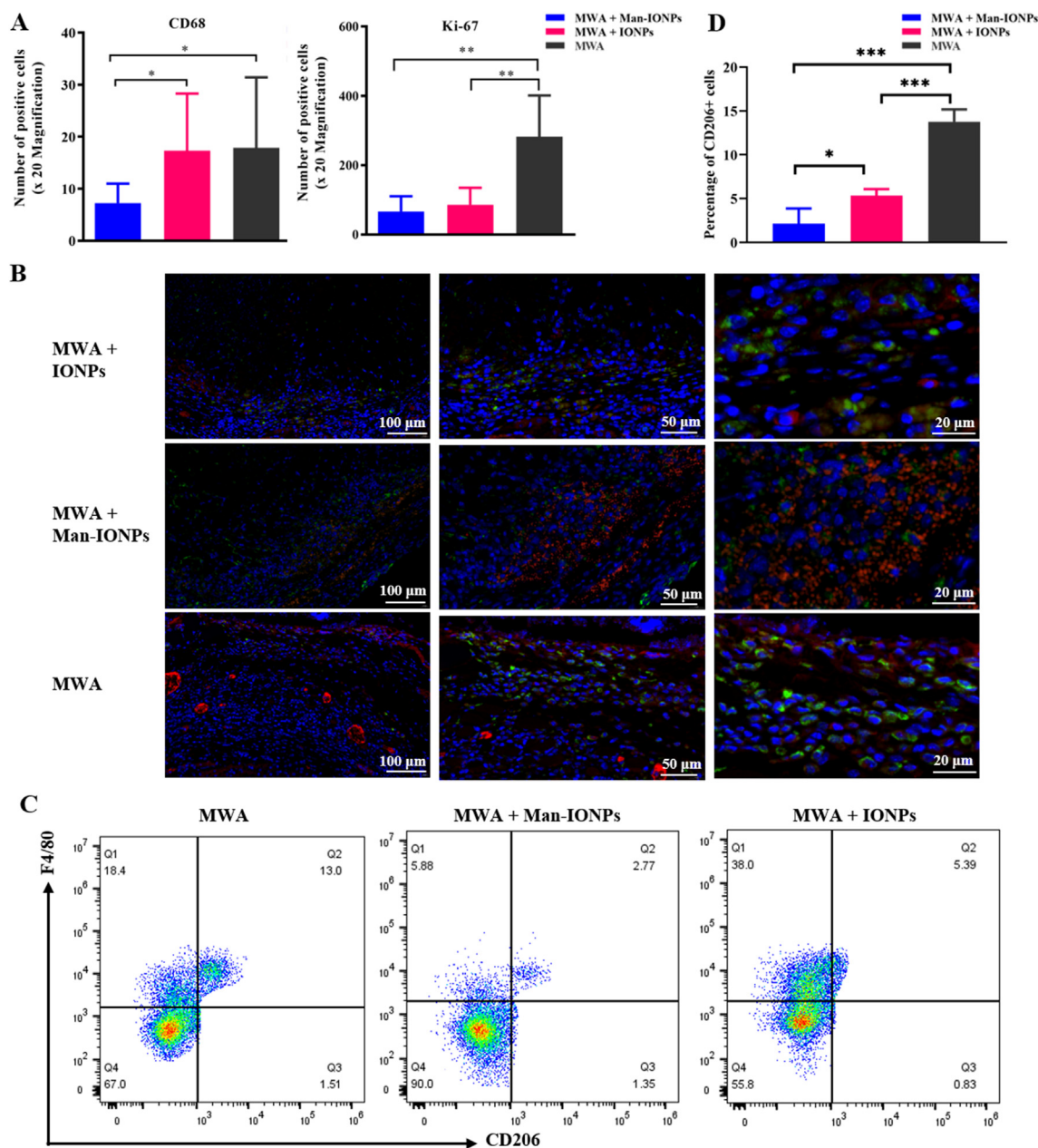


Figure 6 MWA-enhanced macrophage infiltration and man-IONP-facilitated polarization of M2-to M1-like macrophages *in vivo*. (A) Quantitative immunohistochemical data of total macrophages (CD68+) and Ki-67⁺ cells infiltrated into the ablation zone after different treatments. Data are expressed as mean \pm SD ($n = 3$); * $P < 0.05$, ** $P < 0.01$. (B) Immunofluorescence staining of all infiltrated macrophages (CD68+, red) and M2-like macrophages (CD206+, green) in the peri-ablation zone after corresponding treatments in different groups. (C) Flow cytometry graph of the infiltration of M2-like macrophages in MWA, MWA + man-IONPs, and MWA + IONPs groups. (D) Statistical analysis of the flow cytometric analysis of the infiltration of M2-like macrophages in different treatment groups. Data are expressed as mean \pm SD ($n = 3$); * $P < 0.05$, *** $P < 0.001$.

focused on this point and evaluated the inhibitory effects of IONPs on tumor progression. To the best of our knowledge, this is the first study to provide evidence of a correlation between macrophage recruitment after thermal ablation and local tumor progression. Theoretically, the tumor microenvironment has a strong influence on the local progression of residual tumors after MWA¹³. However, unlike typical tumors, residual tumors in the peri-ablation zone are surrounded by an aseptic inflammatory environment due to ongoing tissue repair⁷. Accumulating

inflammatory cells aggravate this microenvironment, with M2 macrophages being an essential component of tissue repair and, therefore, playing a vital role in promoting residual tumor progression after thermal ablation^{33,34}. Using a mouse model of liver cancer with incomplete ablation, we demonstrated that macrophage infiltration increased 2 weeks post-ablation, with a significant elevation in the number of M2 macrophages and Ki-67-positive cells. Therefore, we considered that tumor progression in the peri-ablation zone is attributed to the pro-proliferative effect

of M2-like macrophages. This finding suggests that reversing M2 macrophages in the peri-ablation zone is extremely important for inhibiting tumor progression after MWA.

Hence, we prepared mannose-chelated IONPs to specifically target M2 macrophages, steering their polarization to M1 and mitigating the post-MWA immunosuppressive tumor microenvironment. We added D-mannose to enhance the M2-targeting ability of IONPs since D-mannose can bind to mannose receptors on M2 macrophages^{35,36} more effectively than other targeting motifs (antibodies or peptides)^{37,38}. Our results showed that man-IONPs exhibited a robust targeting effect without compromising their biological safety. Moreover, man-IONPs were superior to IONPs at the same Fe concentration in terms of M2-to-M1 polarization and inhibiting tumor progression. Therefore, M2-targeting IONPs have the potential to outperform the traditional IONPs in tumor inhibition.

The mechanism of the polarization effect of IONPs on M2 macrophages has been explored in several studies. According to a recent review³⁹, two main molecular mechanisms can explain the polarization effect of IONPs: 1) the production of ROS and modulation of redox-sensitive signaling pathways; and 2) the direct engagement and activation of immune response-related receptors such as Toll-like receptors inducing transcriptional reprogramming in macrophages.

We selected IONPs to combine with MWA because of their versatility and feasibility in clinical transformation. To date, IONPs are the only type of nanoparticles that are considered safe for clinical practice. Fridex, Resovist, and Feraheme have been approved by the US Food and Drug Administration (FDA) for clinical diagnosis and treatment. When IONPs inhibit tumors *via* their polarization effect on macrophages, a potential pitfall worth of attention is involved. Liver resident macrophages can also express M2-like markers; thus, IONPs may polarize them to M1-like macrophages. Because macrophages represent a key cellular component of the liver⁴⁰, it cannot rule out that this polarization effect will break the homeostasis in liver tissue. However, in our acute toxicity assay, there were no observed abnormalities in the hepatic tissue and biochemical indicators of mice injected with man-IONPs. Thus, we considered that in the Fe content of 20 mg/kg, even if man-IONPs polarize M2-type liver macrophages to M1-like macrophages, it is not enough to cause other side effects.

In addition, to maximize the combined effect, other functions of IONPs should be explored. Fe-based nanoparticles, used as MRI contrast agents, exhibit maximum visibility in imaging results^{21,27}. Moreover, because of their high heat conductivity and energy transformation efficiency, IONPs are expected to mediate temperature increase during MWA treatment of HCCs¹⁶. This mediation may augment the treatment outcome and inflammation associated with macrophage recruitment, akin to the cavitation-mediated improvement of energy utilization efficiency during physical treatment^{41–43}. Combining several functions of IONPs with MWA will promote innovative research.

5. Conclusions

Our study validated the macrophage polarization effects of man-IONPs and demonstrated their effectiveness in inhibiting local tumor progression in a mouse model of liver cancer. Man-IONPs mitigated residual tumor progression after MWA treatment, decreased the proportion of M2 macrophages, and limited immunosuppression in the peri-ablation zone. Therefore, we propose that

combining man-IONPs with MWA is potential to be a novel strategy for liver cancer treatment.

Acknowledgments

This work was supported by the National Natural Science Foundation of China (Grant Nos. 91859201, 92159305, 81971625, and 82030047).

Author contributions

Rui Cui, Jie Yu, Ping Liang and Long-Fei Tan proposed and designed the project. Rui Cui wrote the manuscript. Rui Cui, Luo Wang, Dongyun Zhang, Jiapeng Wu and Yixuan Zhang conducted the experiments. Rui Cui, Luo Wang and Dongyun Zhang analyzed the results and generated the figures. Jianping Dou and Linan Dong assisted with the animal experiments. Kun Zhang and Jie Yu critically revised and commented on the manuscript. All the authors read and approved the final manuscript.

Conflicts of interest

The authors have no conflicts of interest to declare.

Appendix A. Supporting information

Supporting data to this article can be found online at <https://doi.org/10.1016/j.apsb.2022.05.026>.

References

1. European Association for the Study of the Liver. EASL Clinical Practice Guidelines: management of hepatocellular carcinoma. *J Hepatol* 2018;**69**:182–236.
2. Forner A, Reig M, Bruix J. Hepatocellular carcinoma. *Lancet* 2018;**391**:1301–14.
3. Chu KF, Dupuy DE. Thermal ablation of tumours: biological mechanisms and advances in therapy. *Nat Rev Cancer* 2014;**14**:199–208.
4. Medhat E, Abdel Aziz A, Nabeel M, Elbaz T, Zakaria Z, Shousha H, et al. Value of microwave ablation in treatment of large lesions of hepatocellular carcinoma. *J Dig Dis* 2015;**16**:456–63.
5. Brunello F, Carucci P, Gaia S, Rolle E, Brunocilla PR, Castiglione A, et al. Local tumor progression of hepatocellular carcinoma after microwave percutaneous ablation: a preliminary report. *Gastroenterol Res* 2012;**5**:28–32.
6. Ahmed M, Kumar G, Moussa M, Wang Y, Rozenblum N, Galun E, et al. Hepatic radiofrequency ablation-induced stimulation of distant tumor growth is suppressed by c-Met inhibition. *Radiology* 2016;**279**:103–17.
7. Rozenblum N, Zeira E, Bulvik B, Gourevitch S, Yotvat H, Galun E, et al. Radiofrequency ablation: inflammatory changes in the peri-ablative zone can induce global organ effects, including liver regeneration. *Radiology* 2015;**276**:416–25.
8. Kumar G, Goldberg SN, Wang Y, Velez E, Gourevitch S, Galun E, et al. Hepatic radiofrequency ablation: markedly reduced systemic effects by modulating periablational inflammation *via* cyclooxygenase-2 inhibition. *Eur Radiol* 2017;**27**:1238–47.
9. Oka T, Ohta K, Kanazawa T, Nakamura K. Interaction between macrophages and fibroblasts during wound healing of burn injuries in rats. *Kurume Med J* 2016;**62**:59–66.
10. Shi L, Wang J, Ding N, Zhang Y, Zhu Y, Dong S, et al. Inflammation induced by incomplete radiofrequency ablation accelerates tumor progression and hinders PD-1 immunotherapy. *Nat Commun* 2019;**10**:5421.

11. Talmadge JE, Donkor M, Scholar E. Inflammatory cell infiltration of tumors: jekyll or Hyde. *Cancer Metastasis Rev* 2007;**26**:373–400.
12. Yeung OW, Lo CM, Ling CC, Qi X, Geng W, Li CX, et al. Alternatively activated (M2) macrophages promote tumour growth and invasiveness in hepatocellular carcinoma. *J Hepatol* 2015;**62**:607–16.
13. Mantovani A, Marchesi F, Malesci A, Laghi L, Allavena P. Tumour-associated macrophages as treatment targets in oncology. *Nat Rev Clin Oncol* 2017;**14**:399–416.
14. Zhang K, Xu H, Jia X, Chen Y, Ma M, Sun L, et al. Ultrasound-triggered nitric oxide release platform based on energy transformation for targeted inhibition of pancreatic tumor. *ACS Nano* 2016;**10**:10816–28.
15. Gao SS, Lin H, Zhang HX, Yao HL, Chen Y, Shi JL. Nanocatalytic tumor therapy by biomimetic dual inorganic nanozyme-catalyzed cascade reaction. *Adv Sci (Weinh)* 2019;**6**:1801733.
16. Fang Y, Li HY, Yin HH, Xu SH, Ren WW, Ding SS, et al. Radiofrequency-sensitive longitudinal relaxation tuning strategy enabling the visualization of radiofrequency ablation intensified by magnetic composite. *ACS Appl Mater Interfaces* 2019;**11**:11251–61.
17. Zanganeh S, Hutter G, Spitler R, Lenkov O, Mahmoudi M, Shaw A, et al. Iron oxide nanoparticles inhibit tumour growth by inducing pro-inflammatory macrophage polarization in tumour tissues. *Nat Nanotechnol* 2016;**11**:986–94.
18. Liu X, Zheng J, Sun W, Zhao X, Li Y, Gong N, et al. Ferrimagnetic vortex nanoring-mediated mild magnetic hyperthermia imparts potent immunological effect for treating cancer metastasis. *ACS Nano* 2019;**13**:8811–25.
19. Yu GT, Rao L, Wu H, Yang LL, Bu LL, Deng WW, et al. Myeloid-derived suppressor cell membrane-coated magnetic nanoparticles for cancer theranostics by inducing macrophage polarization and synergizing immunogenic cell death. *Adv Funct Mater* 2018;**28**:1801389.
20. Zhang K, Fang Y, He Y, Yin H, Guan X, Pu Y, et al. Extravascular gelation shrinkage-derived internal stress enables tumor starvation therapy with suppressed metastasis and recurrence. *Nat Commun* 2019;**10**:5380.
21. Zhao J, Zhang Z, Xue Y, Wang G, Cheng Y, Pan Y, et al. Antitumor macrophages activated by ferumoxytol combined or surface-functionalized with the TLR3 agonist poly(I:C) promote melanoma regression. *Theranostics* 2018;**8**:6307–21.
22. Kang H, Kim S, Wong DSH, Jung HJ, Lin S, Zou K, et al. Remote manipulation of ligand nano-oscillations regulates adhesion and polarization of macrophages *in vivo*. *Nano Lett* 2017;**17**:6415–27.
23. Velez E, Goldberg SN, Kumar G, Wang YG, Gourevitch S, Sosna J, et al. Hepatic thermal ablation: effect of device and heating parameters on local tissue reactions and distant tumor growth. *Radiology* 2016;**281**:782–92.
24. Yue W, Chen L, Yu L, Zhou B, Yin H, Ren W, et al. Checkpoint blockade and nanosonosensitizer-augmented noninvasive sonodynamic therapy combination reduces tumour growth and metastases in mice. *Nat Commun* 2019;**10**:2025.
25. Kigerl KA, Gensel JC, Ankeny DP, Alexander JK, Donnelly DJ, Popovich PG. Identification of two distinct macrophage subsets with divergent effects causing either neurotoxicity or regeneration in the injured mouse spinal cord. *J Neurosci* 2009;**29**:13435–44.
26. Hou Y, Zhu L, Tian H, Sun HX, Wang R, Zhang L, et al. IL-23-induced macrophage polarization and its pathological roles in mice with imiquimod-induced psoriasis. *Protein Cell* 2018;**9**:1027–38.
27. Villalta SA, Rinaldi C, Deng B, Liu G, Fedor B, Tidball JG. Interleukin-10 reduces the pathology of mdx muscular dystrophy by deactivating M1 macrophages and modulating macrophage phenotype. *Hum Mol Genet* 2011;**20**:790–805.
28. Wang Z, Liu C, Zhao Y, Hu M, Ma D, Zhang P, et al. Photomagnetic nanoparticles in dual-modality imaging and photo-sonodynamic activity against bacteria. *Chem Eng J* 2019;**356**:811–8.
29. Lu YJ, Chuang EY, Cheng YH, Anilkumar TS, Chen HA, Chen JP. Thermosensitive magnetic liposomes for alternating magnetic field-inducible drug delivery in dual targeted brain tumor chemotherapy. *Chem Eng J* 2019;**373**:720–33.
30. Zhang K, Cheng Y, Ren W, Sun L, Liu C, Wang D, et al. Coordination-responsive longitudinal relaxation tuning as a versatile MRI sensing protocol for malignancy targets. *Adv Sci (Weinh)* 2018;**5**:1800021.
31. Wan J, Wu W, Chen Y, Kang N, Zhang R. Insufficient radiofrequency ablation promotes the growth of non-small cell lung cancer cells through PI3K/Akt/HIF-1 α signals. *Acta Biochim Biophys Sin (Shanghai)* 2016;**48**:371–7.
32. Dong S, Kong J, Kong F, Kong J, Gao J, Ji L, et al. Sorafenib suppresses the epithelial-mesenchymal transition of hepatocellular carcinoma cells after insufficient radiofrequency ablation. *BMC Cancer* 2015;**15**:939.
33. Hanahan D, Weinberg RA. The hallmarks of cancer. *Cell* 2000;**100**:57–70.
34. Condeelis J, Pollard JW. Macrophages: obligate partners for tumor cell migration, invasion, and metastasis. *Cell* 2006;**124**:263–6.
35. Allavena P, Chieppa M, Bianchi G, Solinas G, Fabbri M, Laskarin G, et al. Engagement of the mannose receptor by tumoral mucins activates an immune suppressive phenotype in human tumor-associated macrophages. *Clin Dev Immunol* 2010;**2010**:547179.
36. Taylor PR, Gordon S, Martinez-Pomares L. The mannose receptor: linking homeostasis and immunity through sugar recognition. *Trends Immunol* 2005;**26**:104–10.
37. Yu SS, Lau CM, Barham WJ, Onishko HM, Nelson CE, Li H, et al. Macrophage-specific RNA interference targeting *via* ‘click’, mannosylated polymeric micelles. *Mol Pharm* 2013;**10**:975–87.
38. Locke LW, Mayo MW, Yoo AD, Williams MB, Berr SS. PET imaging of tumor associated macrophages using mannose coated 64Cu liposomes. *Biomaterials* 2012;**33**:7785–93.
39. Mulens-Arias V, Rojas JM, Barber DF. The use of iron oxide nanoparticles to reprogram macrophage responses and the immunological tumor microenvironment. *Front Immunol* 2021;**12**:693709.
40. Krenkel O, Tacke F. Liver macrophages in tissue homeostasis and disease. *Nat Rev Immunol* 2017;**17**:306–21.
41. Chen J, Luo H, Liu Y, Zhang W, Li H, Luo T, et al. Oxygen-self-produced nanoplatfor for relieving hypoxia and breaking resistance to sonodynamic treatment of pancreatic cancer. *ACS Nano* 2017;**11**:12849–62.
42. Zhang K, Li P, Chen H, Bo X, Li X, Xu H. Continuous cavitation designed for enhancing radiofrequency ablation *via* a special radiofrequency solidoid vaporization process. *ACS Nano* 2016;**10**:2549–58.
43. Zhang K, Xu H, Chen H, Jia X, Zheng S, Cai X, et al. CO₂ bubbling-based ‘nanobomb’ system for targetedly suppressing Panc-1 pancreatic tumor *via* low intensity ultrasound-activated inertial cavitation. *Theranostics* 2015;**5**:1291–302.